INSTITUTE OF PHYSICS PUBLISHING JOURNAL OF PHYSICS: CONDENSED MATTER

J. Phys.: Condens. Matter **16** (2004) S5437–S5448 PII: S0953-8984(04)77387-7

Fluidity of water and of hydrated ions confined between solid surfaces to molecularly thin films

Jacob Klein[1,2], **Uri Raviv**[2,4], **Susan Perkin**[1], **Nir Kampf**[2], **Liraz Chai**[2] **and Suzanne Giasson**[3]

[1] PTCL, University of Oxford, Oxford OX1 3QZ, UK
[2] Weizmann Institute of Science, Rehovot 76100, Israel
[3] Département de Chimie, Université de Montréal CP 6128, Montréal, QC, H3C 3J7, Canada
[4] MRL, University of California at Santa Barbara, CA 93106, USA

E-mail: jacob.klein@chem.ox.ac.uk or jacob.klein@weizmann.ac.il

Received 4 March 2004
Published 29 October 2004
Online at stacks.iop.org/JPhysCM/16/S5437
doi:10.1088/0953-8984/16/45/008

Abstract

In contrast to non-associating liquids such as oils or organic solvents, whose viscosity diverges when they are confined by solid surfaces to films thinner than about ten molecular diameters, recent studies reveal that salt-free water remains fluid, with a viscosity close to its bulk value, even when confined to films down to only one or two monolayers thick. For the case of high concentration aqueous salt solutions compressed down to subnanometre films between confining planar surfaces, the hydration sheaths about the ions (trapped between the oppositely charged surfaces) also remain extremely fluid: this behaviour is attributed to the tenacity of water molecules in the hydration layers together with their rapid relaxation/exchange time. Related experiments on highly compressed, polyelectrolyte brushes in aqueous media reveal a remarkable lubricity which is in large measure attributed to similar hydration layers about the charged segments: this water of hydration strongly resists being squeezed out, but at the same time it may rapidly exchange with adjacent water molecules, thereby remaining quite fluid and acting as a molecular lubricant.

1. Introduction

Properties of liquids that are confined to thin films between confining solid surfaces are important in many areas, both in technology and in living organisms. The former include issues of tribology and lubrication, where organic liquids are often used as lubricants, while water in highly confined pores is found in applications involving oil recovery from natural reservoirs, mining, catalysis and corrosion inhibition. Water is also found in confined geometries in porous materials such as Vycor glass, silica gel and zeolites as well as in polymer gels, clays,

rocks, sandstones, micelles, vesicles and microemulsions. In biological systems water is the natural solvent, and highly confined water clearly influences the rates and effectiveness of processes such as the transport of materials and energy in the cell, enzymatic activity of proteins, biochemical reactions and the function of membranes, as well as transport through ion channels and the final rate of approach of interacting molecular species (e.g. ligand–receptor).

The effective viscosity of oils and of other non-associating liquids, such as organic solvents, when compressed between solid surfaces to film thicknesses of less than some 5–8 molecular layers, tends to increase sharply as the film thickness decreases [1]. This can happen either gradually if the molecules are asymmetric, as for the case of liquids consisting of chain-like molecules [1], or more abruptly—at some given confinement—for liquids consisting of simple quasi-symmetric molecules (such as cyclohexane or OMCTS) [2]. In such cases the confined liquid, upon being sheared, becomes capable of sustaining a yield stress for macroscopic periods, thereby behaving as a solid (albeit one whose yield stress may be much weaker than for the corresponding bulk crystal [3, 4]).

The properties of water confined to microscopic and nanoscopic pores or to surfaces have been studied extensively [5], using NMR [6, 7], dielectric relaxation spectroscopy [8, 9], neutron diffraction [10], neutron scattering [7, 11], neutron and x-ray reflectometry [12, 13] simulations [7, 14], and surface force balance (SFB) methods where the water is confined between surfaces in a known and controllable geometry [15–17]. Recently we used an SFB method to study the fluidity of water when it was confined to films of thickness in the range 3–0 $\pm$ 0.3 nm, i.e. from about ten down to at most one or two molecular layers [18, 19]. This was done both for salt-free water and at high salt concentrations, as described below.

2. Surface force balance (SFB) studies of highly confined water

In the SFB method two molecularly smooth, curved mica surfaces (mean radius of curvature R) interact with each other, and the normal and especially shear forces between them may be measured with great sensitivity and with ångström-level resolution as a function of their separation D [2]. The schematic configuration is shown in figure 1. The fluidity or effective shear viscosity of water confined between the surfaces can be measured either by observing the shear forces transmitted across the water in the gap as one of the confining surfaces slides past the other, or by analysing the time over which the two surfaces jump into contact under attractive van der Waals forces. Such jumps occur as follows: the mica surfaces lose K^+ ions to the water, and become negatively charged; as the surfaces approach each other from far apart, the osmotic pressure of the counterions and co-ions between them leads to long ranged repulsion, as predicted by DLVO theory and as shown in figure 2. At a separation of $D =$ ca 3.5$\pm$ca 1 nm the trapped counterions—in the absence of added salt these are predominantly hydrated protons—condense onto and neutralize the negatively charged surfaces, and the van der Waals forces then dominate and pull the surfaces into adhesive contact. We note that these experiments were carried out using both melt-cut mica and torn-off (non-melt-cut) mica, figure 2, to confirm the absence of any nanoparticulate contaminants on the surfaces[5] [21].

The jumps into contact were observed and analysed. It can be shown [19] that if the surfaces jump together spontaneously under van der Waals attraction from a distance D_j to a distance D_0 over a time τ_j, then the effective viscosity is given by the following expression:

$$\tau_j(\eta_{eff}, D_j, D_0) = (18\pi R\eta_{eff}/A)[(D_j^2) - (D_0^2)] \quad (1)$$

[5] Extensive presence of Pt nanoparticles has recently been reported on melt-cut mica surfaces in some laboratories [20] but this can be readily avoided by proper procedures, as described in detail in [21], and as is standard practice in our lab (reference [19] and [22]).

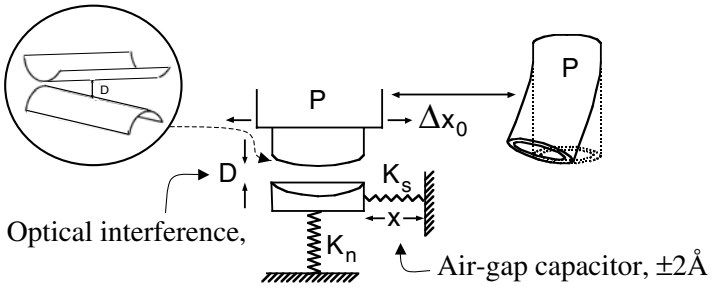

Figure 1. A schematic illustration of the surface force balance (SFB) [2]. The molecularly smooth mica surfaces (top left inset) are glued onto cylindrical lenses (radius 1 cm) and mounted in a crossed-cylinder configuration as shown. The distance D between them (and the bending of the normal spring K_n) is measured with an accuracy of ±1–3 Å using white light interferometry (see figure 3 for typical interference fringes), while the shear motion (and the bending of the shear spring K_s) is measured using an air–gap capacitor to ± ca 2 Å. The relative motion of the surfaces in the normal (ΔD) and shear (Δx) directions may be either finely controlled via a sectored piezoelectric tube as indicated, or—in the case of normal motion—allowed to change slowly via thermal drift. In both cases the normal and shear forces between the surfaces are, respectively, monitored via the bending of the orthogonal springs K_n and K_s to which the cylindrical lenses are attached.

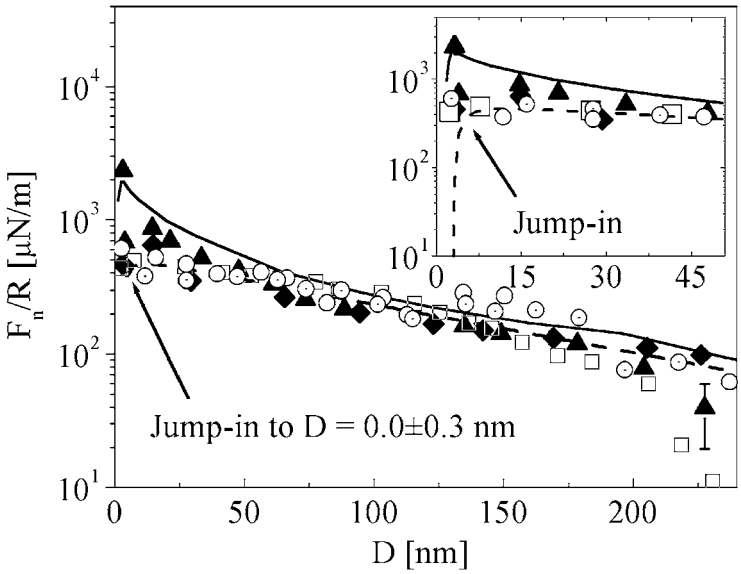

Figure 2. Normal force (F) versus distance profiles between curved mica surfaces in salt-free water (pH = 6.0–6.2), where the force axis is normalized as F/R (R—mean radius of curvature of the mica, ≈1 cm) to yield the interaction energy per unit area between flat plates within the Derjaguin approximation. Different symbols indicate different sets of experiments, with all measurements being taken during compression. In particular, the round symbols (both empty and dotted) are from force profiles obtained with torn-off mica (as opposed to melt-cut mica, all other symbols; the error bar shown is representative, others being left out for the sake of clarity). From $D = 3.5 \pm 1$ nm, there was a jump in to adhesive flat contact at D_0. The solid curve corresponds to the results of earlier studies by Pashley [38]. The dashed curve is the best fit of the linear parts of the profiles to a DLVO expression. The inset shows the forces over the last 50 nm in more detail (adapted from [19]).

where η_{eff} is the effective mean viscosity in the gap $\{D_j, D_0\}$ and A is the Hamaker constant between the mica surfaces across water.

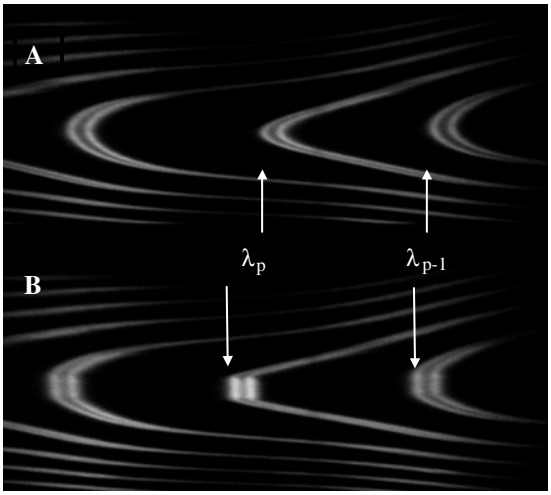

Figure 3. A typical set of fringes of equal chromatic order (FECO) observed during an SFB experiment: (A) with the mica surfaces 31.1 nm apart and (B) following the jump to adhesive contact, when the glue layers supporting the mica sheets flatten under the attractive van der Waals forces between the surfaces. The fringes shown are for mica sheets interacting across air, but similar fringes are observed with liquid between the surfaces. Using high speed video-microscopy it is possible to follow the changes in wavelengths λ_p and λ_{p-1} of adjacent fringes of order p, $p-1$, during the jump together of the surfaces.

In figure 3 is shown a set of optical interference fringes typical of those observed in the SFB experiments, whose shape and wavelengths reveal the geometry of interaction and the separation D between them. In figure 3(A) the fringes are shown prior to the surfaces jumping into contact, and in figure 3(B), following the jump in: here the strong adhesive forces between the surfaces have caused the glue layer underlying the mica sheets to flatten. In the earlier measurements [18, 19] the time τ_j for the jump into contact was estimated to be in the range 0.2–0.5 s, and a summary of the data is shown in figure 4. The top rhs cartoon in figure 4 shows schematically the geometry of the curved surfaces jumping into contact, and the lower rhs inset shows the theoretically predicted times for jumps from a surface separation D_j to contact (equation (1)). The shaded band of data in the main figure is the range of jump times τ_j estimated from the experiments. As noted above, τ_j is related to the effective viscosity η_{eff} of the water being squeezed out from between the approaching surfaces (y-axis in figure 4) by equation (1); the mean value of η_{eff} evaluated from this equation is close to that of bulk water, as shown by the arrow on the viscosity axis in figure 4. The analysis leading to equation (1) and the values of the viscosity in figure 4 is based on the assumption of a stick boundary condition of the water at the confining mica surfaces, which may not hold strictly at sufficiently high shear rates [23]. An extension of this analysis shows [24], however, that allowing for slip at the mica surface does not significantly change our conclusion that the effective viscosity of the water in the gap remains close to its bulk value. From measurements similar to those shown in figure 4, we have also shown [24] that the viscosity of water confined to nanometre and subnanometre films by *hydrophobic* surfaces—where slip of water at the surface is known to occur—is also within an order of magnitude or so of its bulk value. More recently [25] fringes such as those in figure 3 were video-imaged prior to and during the jump into contact, and the jump dynamics analysed in detail. These measurements confirm quantitatively the earlier estimates for τ_j appearing in figure 4.

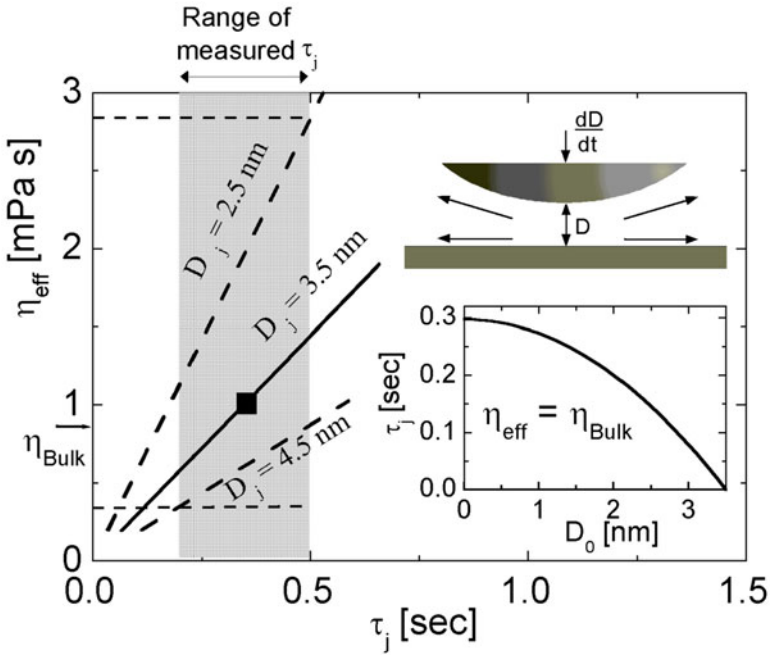

Figure 4. Evaluating the effective viscosity of water confined to subnanometre films. The cartoon (top right) illustrates the jump in driven by van der Waals attraction and opposed predominantly by the hydrodynamic force resulting from the expulsion of the viscous liquid from between the surfaces. The inset (lower right) shows how, for an effective viscosity $\eta_{\text{eff}} = \eta_{\text{bulk}} = 0.86$ mPa s (the viscosity of bulk water at 23 °C), the jump time τ_{j} is predicted (equation (1)) to vary with jump distance for a jump commencing at $D_{\text{j}} = 3.5$ nm. The main figure shows the effective viscosity η_{eff} (of the squeezed-out water) corresponding to the jump time to contact τ_{j}, based on equation (1), for three values of the jump distance D_{j}: the mid-range value 3.5 nm (solid line) and the two extremes from which jumps occurred, $D_{\text{j}} =$ ca 2.5 and 4.5 nm (broken lines). The shaded vertical band is the range of experimentally estimated τ_{j}, showing that the mid-range value of the effective viscosity η_{eff} (with respect to the scatter in D_{j} and τ_{j}), indicated as a solid square, is close to η_{bulk} itself (adapted from [18, 19]).

This behaviour—where the fluidity of water confined down to subnanometre films remains comparable with its bulk value—is at first sight unexpected and is in sharp contrast to the case for non-associating liquids, which tend to become solid-like under equivalent confinement, as noted earlier [1, 2]. We attribute this to the different phase density behaviour for water compared to most non-associating (especially organic) liquids, as illustrated and explained in figure 5. Essentially, it is due to the van der Waals fields in the close vicinity of the solid surfaces, which act to attract and thereby densify liquids adjacent to the surfaces. Such densification acts in very different ways for non-associating liquids and for water. In the former case, the increase in density in the confined liquid tends to make it more solid-like [26], since the solid phase is denser than the liquid phase. For water, however, a similar densification near the surfaces does not lead to solid-like behaviour. The reason for this may be viewed at different levels of sophistication (though detailed models have not yet been developed), but it essentially arises, we believe, because solid water (ice) is less dense than liquid water: thus the densification of the water within the gap *suppresses* its tendency to become solid-like. An alternative way of looking at this is to consider that the solid, confining surfaces prefer the denser liquid phase in their immediate vicinity as the overall van der Waals interaction energy is then lower. Very recently a computer simulation of a liquid which dilates on solidifying (much as water does)

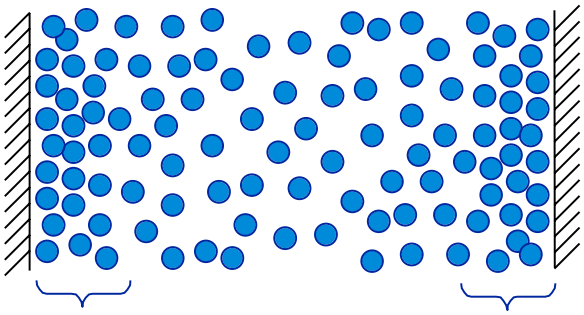

Figure 5. Illustrating schematically the proposed origin for the persistent fluidity of highly confined water in contrast to the solid-like behaviour of similarly confined non-associating liquids. At large separations the molecules in the central region of the gap are at their liquid-like density, while the molecules in the near-surface regions (bracketed) are attracted to the respective surfaces by van der Waals forces, equivalent to an effective pressure, and are therefore densified. As the surfaces approach, the two densified (bracketed) regions overlap and the mean density in the gap increases: this promotes solidification for non-associating liquids (as described in [1]), but tends to suppress it for the water, in line with the different phase behaviour of the latter, since liquid water is denser than ice.

(This figure is in colour only in the electronic version)

indicated that such a liquid remains fluid under all compressions between two solid walls, in line with our findings [27].

While the behaviour of salt-free water in extreme confinement is of considerable interest, it is important to know how confined water behaves at high salt concentrations, as in most biological systems. When salt is added to high concentrations to the water, up to 0.1 M NaCl—concentrations typical of biological systems—the forces across the resulting aqueous electrolyte solutions under compression and shear are very different to those across salt-free water shown above (figure 2). In these conditions of high added salt, as the two charged (mica) surfaces approach from large separations, there are still trapped counterions between them (to compensate the negative surface charges). However, in contrast to the no-added-salt case above (figure 2), these are now predominantly hydrated Na^+ ions (very similar results were obtained also with K^+ ions). These ions hold on to their hydration sheath very tenaciously when compressed by the charged surfaces, so they do not readily condense into the negatively charged lattice sites to neutralize the mica surfaces. The result is that, rather than a jump into contact under the van der Waals attraction, a strong so-called hydration repulsion dominates [28], even at pressures of many atmospheres, comparable with pressures pertaining in living systems. This is shown in figure 6. We found [29] that when two mica surfaces were strongly compressed and sheared within the hydration repulsion regime, the frictional drag between them was extremely small, as shown in figure 7. It corresponds to effective friction coefficients μ_{eff} (defined as $\mu_{\text{eff}} =$ [force to slide]/[normal load]) that were smaller than about 0.0002 in the conditions of our experiments[6]. This extreme fluidity of the hydration sheaths, combined at the same time with the difficulty of squeezing them out from between the compressing surfaces, results in a combination leading to remarkable lubricity. We attribute the origin of this as follows, as also illustrated in figure 8.

Although the hydration sheaths are tenaciously attached to the ions and so are not readily squeezed out from between the surfaces even under substantial compression, the water

[6] While the results shown in figures 6 and 7 were obtained using melt-cut mica, identical results [22] were obtained when using mica prepared by tearing rather than melt-cutting, showing again—as in figure 2—that Pt nanoparticles (see footnote 5) had no effect on our results.

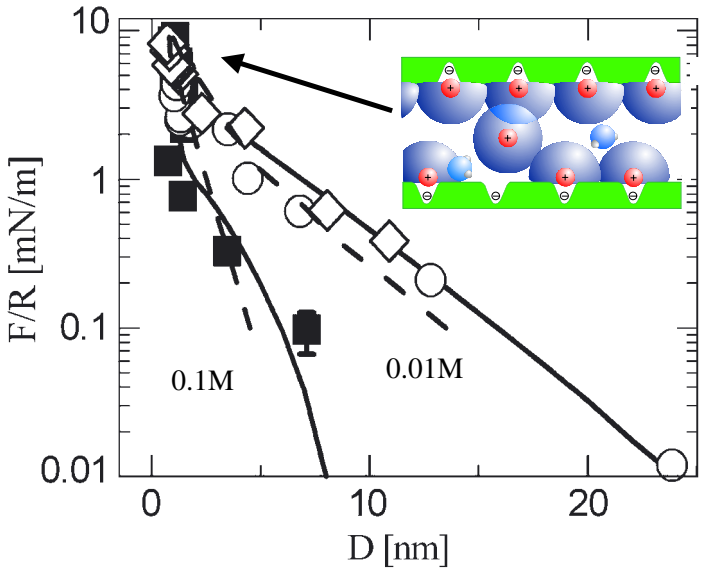

Figure 6. The normal force versus distance profile between mica surfaces across aqueous NaCl solutions, at the two concentrations shown, normalized with respect to the radius R as in figure 2. For clarity, only a single (representative) error bar is shown. The cartoon illustrates the origin of the repulsion by trapped hydrated ions in the hydration repulsion regime indicated by the arrow. The dashed and continuous curves are, respectively, the literature profiles from earlier studies [16], and a fit to the present data using double-layer interactions augmented by hydration repulsion (adapted from [29]).

molecules within the sheaths are known to exchange rapidly with other water molecules, at a rate which depends on the ions, but which for monovalent ions such as Na^+ and K^+ is of order 10^9 s^{-1} in the bulk [30]. Therefore as long as the shear rate $\dot{\gamma}$ of the confined film, given by (v_s/D), is significantly smaller than this, we believe that the frictional drag between the shearing surfaces will be extremely small. This is because the hydration sheaths—despite their great reluctance to be squeezed out—must behave in a very fluid manner at shear rates that are very much lower than their relaxation rates (the latter are comparable to the hydration water exchange rates), as might be expected on general grounds for fluids undergoing deformation. It is of interest to estimate the effective 'shear viscosity' $\eta'_{\rm eff}$ of the hydrated ions, which may be done (assuming stick boundary conditions) using the Newtonian relation equating the shear stress to the product of $\eta'_{\rm eff}$ and the shear rate. When this is done [29] an upper limit is obtained for $\eta'_{\rm eff}$ of about 0.1 Pa s, a value some 100-fold higher than that of bulk water. We stress that this is an *upper limit* arising from the fact that the actual shear force measured during sliding in the hydration repulsion regime (figure 7, traces c–e) is so small as to be within the scatter in the data, and the actual value may be smaller still. However, strictly speaking this is not a 'real' shear viscosity, since the hydrated ions are not free to squeeze out of the gap, even under large compressions. This combination of sustaining large normal load (when trapped between charged surfaces) together with high fluidity under shear—which reduces the effective friction between the sliding surfaces remarkably—makes the behaviour of such hydrated ions very similar to that of molecular ball bearings. We believe that the role of hydrated ions in providing such fluid—yet tenaciously held—sheaths may be of importance more generally in interactions in biological systems, as well as in aqueous systems in a non-biological context as discussed below.

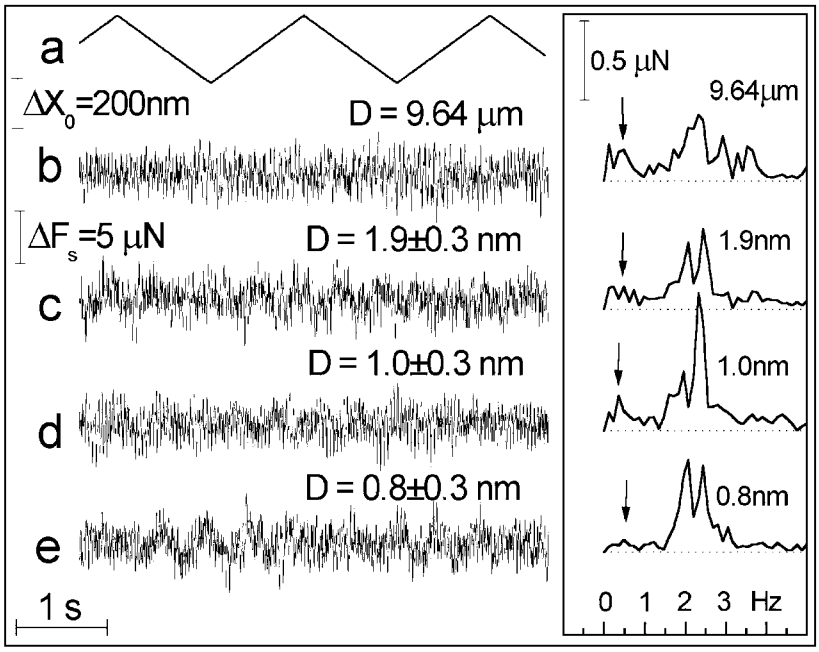

Figure 7. Traces of applied motion of the top mica surface (trace a, where Δx_o is the lateral motion applied to the top mica surface) and of corresponding forces transmitted to the lower mica surface (traces b–e, where ΔF_s is the shear force transmitted to the lower surface across the liquid in the gap) when the two are a distance D apart as indicated by the traces, separated by aqueous NaCl solutions at about 0.1 M (traces c, e) and about 0.01 M (traces b, d) concentrations. The normal forces between the surfaces are those corresponding to the normal force–distance profile (as in figure 6) at the respective D values shown. The rhs shows the corresponding frequency analyses of the transmitted forces, with arrows pointing to the transmitted force at the drive frequency. The shear forces in the hydration repulsion regime—traces c–e—are, within the scatter, equal to those when the surfaces are far apart (trace b). This shows the extreme fluidity of the hydrated ions under shear, despite their ability to support a large normal load (adapted from [29]).

As an example of this, the fluidity of the confined hydration layer described above has been implicated in reducing friction in a rather different system: that between compressed polyelectrolyte brushes as they slide past each other. Such charged flexible polymers (though not necessarily having the brush configuration) are ubiquitous in biological systems, and shear at protein surfaces—which have charged patches—may also be mediated in a similar fashion. Using an SFB, it was recently shown [31] that the effective friction between charged polymer brushes was very significantly lower than that between sliding compressed neutral brushes at comparable compressions and shear rates, when normalized to the volume fraction of the highly compressed chains. A summary of these results is shown in figure 9. This shows the effect of different polymeric surfactants in modifying the friction: the differences between neutral brushes [32, 33] and neutral adsorbed chains [34] and charged brushes [31] on the one hand, and between charged, adsorbed polymers [25] and charged brushes on the other, suggests an origin for this behaviour. The configuration is illustrated schematically in figure 10.

We attribute the extremely low friction afforded by such brushes to two main effects. The first is the reluctance of each chain within a given brush to penetrate into the opposing layer, an effect well known also for neutral brushes [33, 35, 36]. This reluctance arises from the excluded volume of the segments in the good-solvent conditions of the interaction, which in

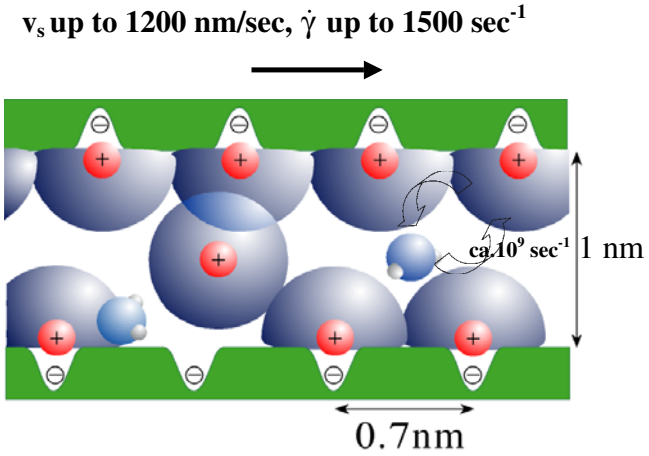

Figure 8. Illustrating schematically the origin of the high fluidity in shear and the resulting lubricity induced by trapped counterions in the hydration repulsion regime as the surfaces slide relative to each other at shear velocities v_s and shear rates $\dot{\gamma}$ in the range indicated. The hydration layers are tenacious with respect to being removed by squeeze-out between the surfaces, but the exchange time for the hydration water is (for monovalent ions [30]) typically 10^{-9} s in the bulk, corresponding to an exchange/relaxation rate of order 10^9 s^{-1} as indicated (though this assumes, without evidence, that the exchange and relaxation rates of the hydration layers will not change significantly under confinement). This is much higher than the maximal shear rates in our experiments, so the layers appear fluid. (The cartoon is roughly to scale: the mean charge separation shown, 7 Å, is to scale with the surface separation $D = 1$ nm, and corresponds to the mean value appropriate for fully ionized mica surfaces that have lost K^+ ions to solution. Water molecules ('oxygen' spheres with two 'hydrogen' hemispheres attached) are also shown roughly to scale (diameter about 2.5 Å), as are the diameters both of the ions (Na^+, diameter about 2 Å) and of the hydration sheaths about them (about 7–8 Å)).

turn results in a strong potential opposing the mutual interpenetration of the brushes. Typically, for compressions that are not too extreme, the extent of interpenetration d for neutral brushes varies very weakly with the intersurface separation D, as $d \propto D^{-1/3}$; that is, an eightfold compression, say, will only double the extent of interpenetration [33, 35, 36]. For the case of charged brushes, the potential opposing interpenetration is moreover augmented relative to that of neutral brushes by the presence of mobile counterions within the brush layers, so mutual interpenetration is suppressed even further. The point is that weak interpenetration results in a sheared zone that is rather narrow and within which the polymer segments are short and unlikely to be entangled with each other: this reduces the dissipation and hence the frictional drag.

A second and important effect is related to the studies described above, and due, we believe, to the hydration layers surrounding each of the charged segments on the ionized polyelectrolytes. The reason for the presence of such hydration sheaths is qualitatively identical to that for hydration layers surrounding simple ions in solution: it arises because the polarizability of the water molecules in the hydration shell enables a significant reduction in the self-energy of the ionic charge. When they are compressed strongly against each other (many atmospheres for the system studied [31]), the opposing charged brushes come into intimate contact; however, the frictional drag between the contacting, hydrated, charged segments at the interface between the two brushes will still be very low. This is because of the fluidity of the tenaciously held hydration sheaths, as discussed in detail above for simple ions. It is from the combination of these effects—both more effective suppression of mutual interpenetration

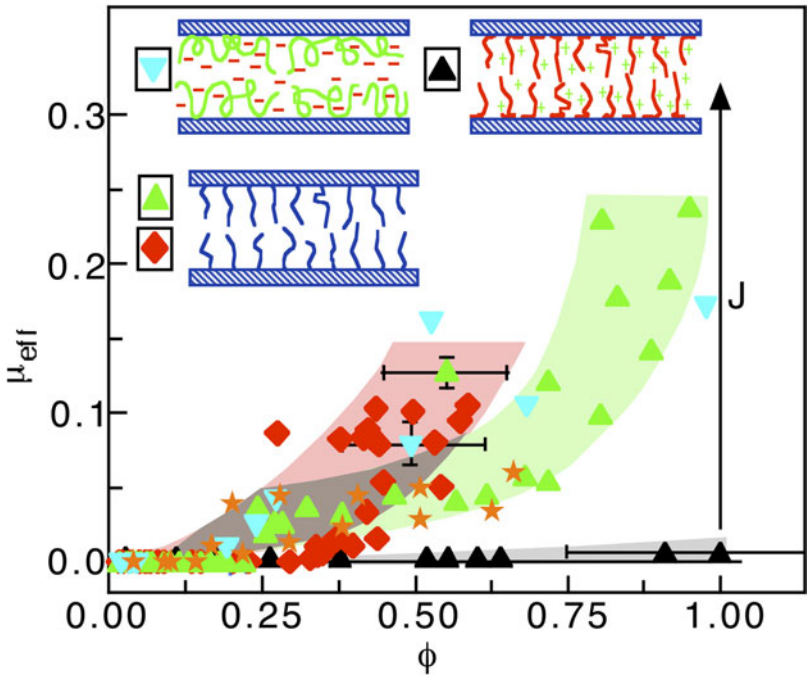

Figure 9. Variation of the effective friction coefficient between mica surfaces bearing different types of polymeric surfactants, as a function of mean surfactant layer volume fraction under compression. Red and green symbols and shaded bands: neutral brushes in organic [32] or aqueous [39] solvents; blue symbols: charged adsorbed polymers [25]; orange stars: adsorbed neutral polymers in aqueous electrolyte solution [34]; black symbols: charged brushes as described in the present study. The arrow marked J indicates the point at which the polyelectrolytes sheared off from the surfaces and the surfaces jumped into adhesive contact marked by a high friction (adapted from [31]).

resulting from the counterion layers, and the lubrication by the fluid hydration shells about the charged segments—that polyelectrolyte brushes provide much more effective friction reduction than their neutral counterparts. The origin of the difference between the charged brushes and the charged *adsorbed* polymers [25], for which both counterions and hydration layers are also present, is different; it may be attributed to the effect of bridging in the latter (such bridging is also expected in neutral adsorbed chains, as shown—orange stars—in figure 9). This occurs when an adsorbing chain attaches simultaneously to both sliding surfaces, so the lateral motion stretches it and then causes it to drag across the surfaces [25, 37]. Such a mechanism can result in additional energy dissipation which manifests itself as higher frictional drag.

3. Conclusions

The results above describe how, in contrast to non-associating liquids, water that is confined to thin films by solid surfaces can retain its fluidity even when the film thickness is reduced to subnanometre levels. Moreover, when the concentration of (monovalent) salts in the aqueous medium is high, hydrated ions are trapped between the charged surfaces due to the need for charge compensation: the hydration sheaths about the ions retain a fluidity under shear, while at the same time they resist being squeezed out from between the compressing surfaces. Our results, at pressures (up to O(10 atm)) and at salt concentrations characteristic of living

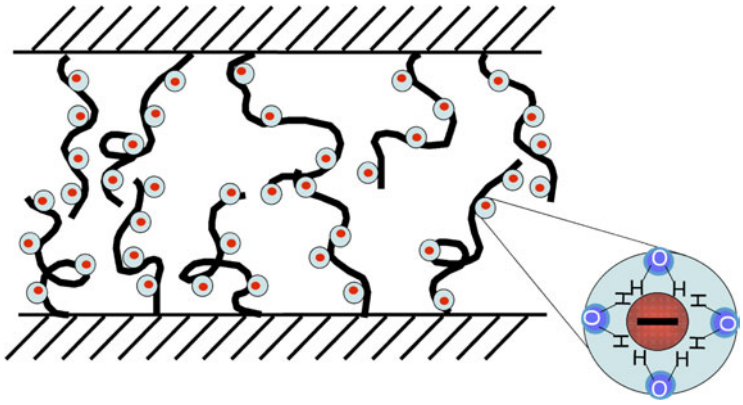

Figure 10. A schematic illustration of two polyelectrolyte brushes compressed against each other. The circles decorating the polymer chains represent ionized segments on the chains, each with a hydration sheath around it, as indicated in the magnified inset on the right (showing the negatively charged segment surrounded by a hydration layer), to which we attribute an important part of the lubricity seen in figure 9. For clarity we have omitted the mobile counterions within the brushes, which are there at a concentration roughly equal to that of the charged segments.

systems, may have interesting implications for lubrication effects in biology. These range from interactions between receptors and ligands, or between fusing cell surfaces—where the final water films a few ångströms thick need to be squeezed out before molecular contact can occur—to sliding of proteins and cells past the extracellular matrix, and to lubrication of mammalian joints and of the cornea. In the model study on rubbing polyelectrolyte brushes described above, the hydration layers are implicated in the striking lubrication achieved, suggesting that their role in regulating frictional drag may be dominant whenever charged species (whether solid surfaces, surfaces of proteins, or charged macromolecues) interact across aqueous media. Current studies are directed at examining in detail the viscosity of water as a function of its confinement, as well as the range of conditions under which hydration sheaths about ions may be utilized as molecular lubrication layers.

Acknowledgments

We thank D Chandler, S Safran, P Pincus and T Witten for discussions. Support by the Eshkol Foundation (studentship to UR), the Deutsche–Israel Program (DIP), the US–Israel Binational Science Foundation, the Minerva Foundation, the Charpak-Vered Fellowship (Canadian Friends of the Weizman Institute) and the EPSRC (UK) is acknowledged with thanks.

References

[1] Gee M L, McGuiggan P M, Israelachvili J N and Homola A M 1990 *J. Chem. Phys.* **93** 1895
Granick S 1991 *Science* **253** 1374
Klein J and Kumacheva E 1995 *Science* **269** 816
[2] Klein J and Kumacheva E 1998 *J. Chem. Phys.* **108** 6996
[3] Gubbins K E, private communication
Gubbins K E 2004 *J. Phys.: Condens. Matter* **16**
[4] Kumacheva E and Klein J 1998 *J. Chem. Phys.* **108** 7010

[5] See papers in Bellissent-Funel M-C and Dore J C (ed) 1994 *Hydrogen Bond Networks* (*NATO ASI Series* vol 435) (Dordrecht: Kluwer–Academic)
[6] Chen S-H and Bellissent-Funel M-C 1994 *Hydrogen Bond Networks* ed M-C Bellissent-Funel and J C Dore (Dordrecht: Kluwer–Academic) p 307
[7] Clifford J 1975 *Water in Disperse Systems* vol 5, ed F Franks (New York: Plenum) p 75
[8] Pissis P *et al* 1994 *Hydrogen Bond Networks* ed M-C Bellissent-Funel and J C Dore (Dordrecht: Kluwer–Academic) p 425
[9] Kremer F 2002 *J. Non-Cryst. Solids* **305** 1
[10] Ricci M A *et al* 2000 *J. Phys.: Condens. Matter* **12** A345
[11] Bellissent-Funel M C, Lal J and Bosio L 1993 *J. Chem. Phys.* **98** 4246
[12] Cheng L *et al* 2001 *Phys. Rev. Lett.* **87** 156103
[13] Williams-Daryn S *et al* 2002 *J. Colloid Interface Sci.* **256** 314
[14] Rossky P J 1994 *Hydrogen Bond Networks* vol 435, ed M-C Bellissent-Funel and J C Dore (Dordrecht: Kluwer–Academic) p 337
[15] Horn R G, Smith D T and Haller W 1989 *Chem. Phys. Lett.* **162** 404
[16] Israelachvili J N 1986 *J. Colloid Interface Sci.* **110** 263
[17] Homola A M *et al* 1989 *J. Tribol.* **111** 675
[18] Raviv U, Laurat P and Klein J 2001 *Nature* **413** 51
[19] Raviv U *et al* 2004 *Langmuir* at press
[20] Heuberger M and Zach M 2003 *Langmuir* **19** 1943
Lin Z and Granick S 2003 *Langmuir* **19** 7061
[21] Israelachvili J N *et al* 2004 *Langmuir* **20** 3616–22
[22] Perkin S *et al* to be published
[23] Bonaccurso E, Kappl M and Butt H J 2002 *Phys. Rev. Lett.* **88** 076103
[24] Raviv U *et al* 2002 *J. Phys.: Condens. Matter* **14** 9275
[25] Kampf N, Raviv U and Klein J 2004 *Macromolecules* **37** 1134
[26] Cui S T, Cummings P T and Cochran H D 2001 *J. Chem. Phys.* **114** 7189
[27] Jagla E A 2002 *Phys. Rev. Lett.* **88** 245504
[28] LeNeveu D M, Rand R P and Parsegian V A 1976 *Nature* **259** 601
Israelachvili J N and Adams G E 1978 *J. Chem. Soc. Faraday Trans.* I **79** 975
Pashley R M 1981 *J. Colloid Interface Sci.* **83** 531
Pashley R M 1982 *Adv. Colloid Interface Sci.* **16** 57
[29] Raviv U and Klein J 2002 *Science* **297** 1540
[30] Cotton F A and Wilkinson G 1998 *Advanced Inorganic Chemistry* (New York: Wiley)
[31] Raviv U *et al* 2003 *Nature* **425** 163
[32] Klein J *et al* 1994 *Nature* **370** 634
[33] Klein J 1996 *Annu. Rev. Mater. Sci.* **26** 581
[34] Chai L and Klein J, to be published
[35] Witten T, Leibler L and Pincus P 1990 *Macromolecules* **23** 824
[36] Wijmans C M, Zhulina E B and Fleer G J 1994 *Macromolecules* **27** 3238
[37] Raviv U, Tadmor R and Klein J 2001 *J. Phys. Chem.* B **105** 8125
[38] Pashley R M 1981 *J. Colloid Interface Sci.* **80** 153
[39] Raviv U *et al* 2002 *Langmuir* **18** 7482